Construction Progress of Chinese First Quasi-axisymmetric Stellarator (CFQS) and Preliminary Results in the CFQS-Test Device

Y. Xu[1*], J. Cheng[1], H. F. Liu[1], X. Q. Wang[1], W. M. Xuan[1], J. Huang[1], H. Liu[1], X. Zhang[1], J. F. Shen[1], J. Hu[1], H. Lan[1], Y.C. Li[1], W. Li[1], H. Zhou[1], J. R. Shao[1], A. Shimizu[2,3], M. Isobe[2,3], S. Okamura[2], M. Shoji[2], K. Ogawa[2,3], H. Takahashi[2,3], H. Yamaguchi[2,3] and D. P. Yin[4]

[1] Institute of Fusion Science, School of Physical Science and Technology, Southwest Jiaotong University, Chengdu 610031, China
[2] National Institute for Fusion Science, National Institutes of Natural Sciences, Toki 509-5292, Japan
[3] The Graduate University for Advanced Studies, SOKENDAI, Toki 509-5292, Japan
[4] Hefei Keye Electro Physical Equipment Manufacturing Co., Ltd, Hefei 230031, China

*Email: xuyuhong@swjtu.edu.cn

Abstract. The Chinese First Quasi-axisymmetric Stellarator (CFQS) is being constructed as an international joint project between Southwest Jiaotong University (SWJTU, China) and National Institute for Fusion Science (NIFS, Japan), aiming to prove the inherent advantages of the quasi-axisymmetric (QA) magnetic configuration in confining plasmas by substantial reduction of neoclassical transport and stabilizing MHD instabilities by a magnetic well structure, etc. The CFQS project is divided into two stages. ***The first one*** focuses on testing of feasibility and accuracy of modular coils for realization of the QA topology, which is conducted on the CFQS-Test (CFQS-T) device and operated at low magnetic field of 0.1 T. ***The second stage*** is scheduled to delve into plasma properties of high parameters at relatively high magnetic field (1 T) in a QA stellarator, for which stronger support structures are needed to withstand large electromagnetic forces. In the paper, the construction progress of CFQS and the preliminary experimental results obtained in the CFQS-T device are outlined.

1. Introduction of CFQS stellarator

It is well-known that conventional stellarators have relatively poor confinement compared with tokamaks due to large neoclassical transport losses caused by radial drifts of localized particles [1]. Theoretical studies suggested that neoclassical transport can be significantly reduced by optimizing the magnetic topology, like quasi-helical, quasi-isodynamic and quasi-toroidal symmetries [2-4]. Based on the quasi-axisymmetric (QA) magnetic geometry, Southwest Jiaotong University (SWJTU, China) has collaborated with National Institute for Fusion Science (NIFS, Japan) since 2017 to design and construct the advanced stellarator — Chinese First Quasi-axisymmetric Stellarator (CFQS) [5, 6]. The QA magnetic geometry offers innovative solutions for confining high-β plasmas by combining the merits of advanced tokamaks and optimized stellarators [7, 8]. The main parameters of CFQS are: the major/minor radius are 1.0 m/0.25 m, the toroidal periodic number is 2 and the magnetic field strength is 1.0 T. The physical design of the CFQS is characterized by several distinctive features [9, 10]: (i) large reduction of neoclassical transport losses by QA configuration; (ii) formation of a magnetic well structure spanning from plasma edge to the core, in favor of suppression of MHD instabilities, (iii) a small aspect ratio which maximizes the plasma volume to sustain high fusion power densities and (iv) lessened toroidal viscosity to boost E×B sheared flows and hence to suppress turbulent transport. Figures 1(a) and (b) depict the Poincaré plot of magnetic flux surfaces in the Boozer coordinates at the toroidal angle $\phi =$

0° and the radial profile of Fourier components of the normalized magnetic field strength ($B_{m,n}/B_{0,0}$) in CFQS. One can see that the dominant components is $B_{1,0}$ which guarantees the QA configuration (n=0). Figure 1(c) further shows that the magnetic well structure and irrational iota (ι) values are beneficial for stabilizing MHD instabilities.

The CFQS project is divided into two stages. *The first one* focuses on testing of feasibility and accuracy of modular coils for realization of the QA topology, which is conducted on the CFQS-Test (CFQS-T) device and operated at low magnetic field of 0.1 T. Shown in Fig. 2 is the photo of CFQS-T installed in the experimental hall of SWJTU in August 2024. *The second stage* is planned to investigate plasma properties of high parameters at relatively high magnetic field (1 T) in a QA stellarator, for which stronger support structures are required to bear large electromagnetic forces.

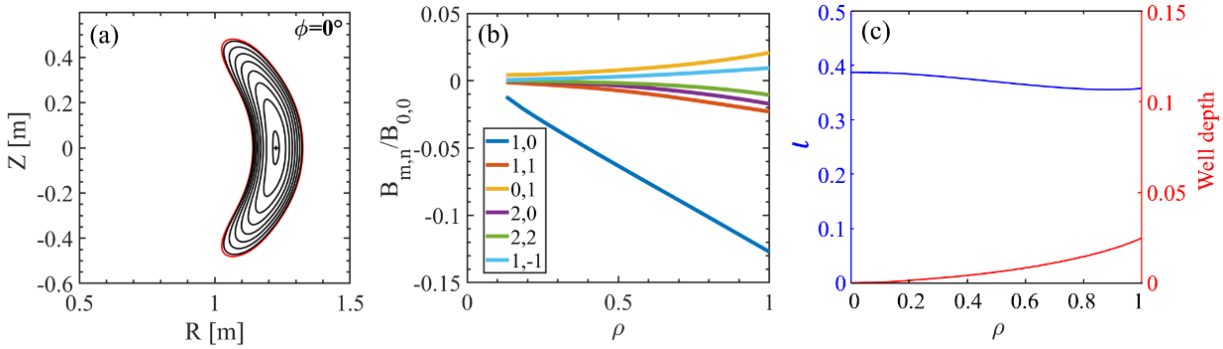

Fig. 1. (a) Poincaré plot of magnetic flux surfaces in Boozer coordinate at $\phi = 0°$, (b) radial profiles of Fourier components of the normalized magnetic field strength ($B_{m,n}/B_{0,0}$) and (c) radial profiles of the rotational transform (ι) and magnetic well in the CFQS stellarator.

2. Progress of CFQS construction

The main body of the CFQS stellarator is shown in Fig. 3, including the coil system (modular coils, toroidal and poloidal field coils), the vacuum vessel, supporting structure (coil cases, center pole and pillars between adjacent coils) and the water cooling pipes [11-13]. **The coil system** consists of 16 non-planar modular coils (MCs), 4 poloidal field coils (PFCs) and 12 toroidal field coils (TFCs). The MCs of four types (MC1, MC2, MC3, MC4) are designed and manufactured to generate the QA magnetic

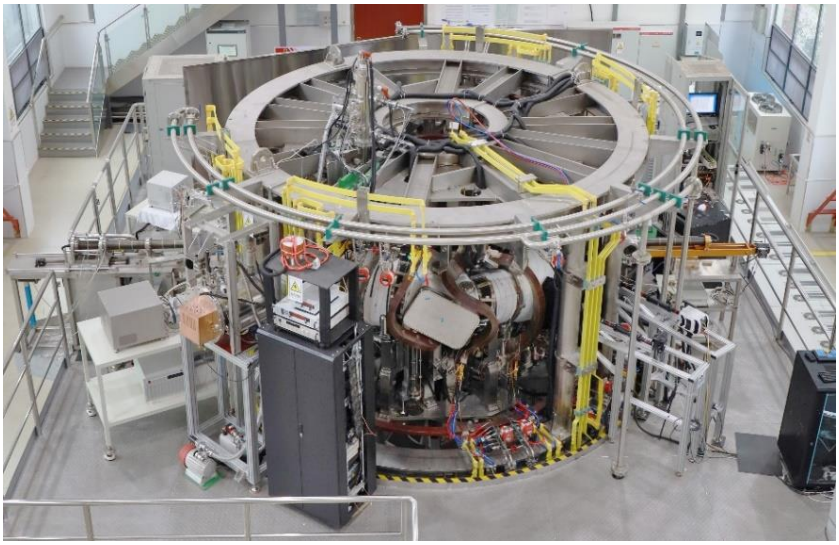

Fig. 2. Photo of CFQS-T in the experimental hall.

configuration. The PFCs are used to control the radial movement of the magnetic axis, and the TFCs for adjusting the iota profile and forming the magnetic island divertors [14]. Among the magnet coils, the

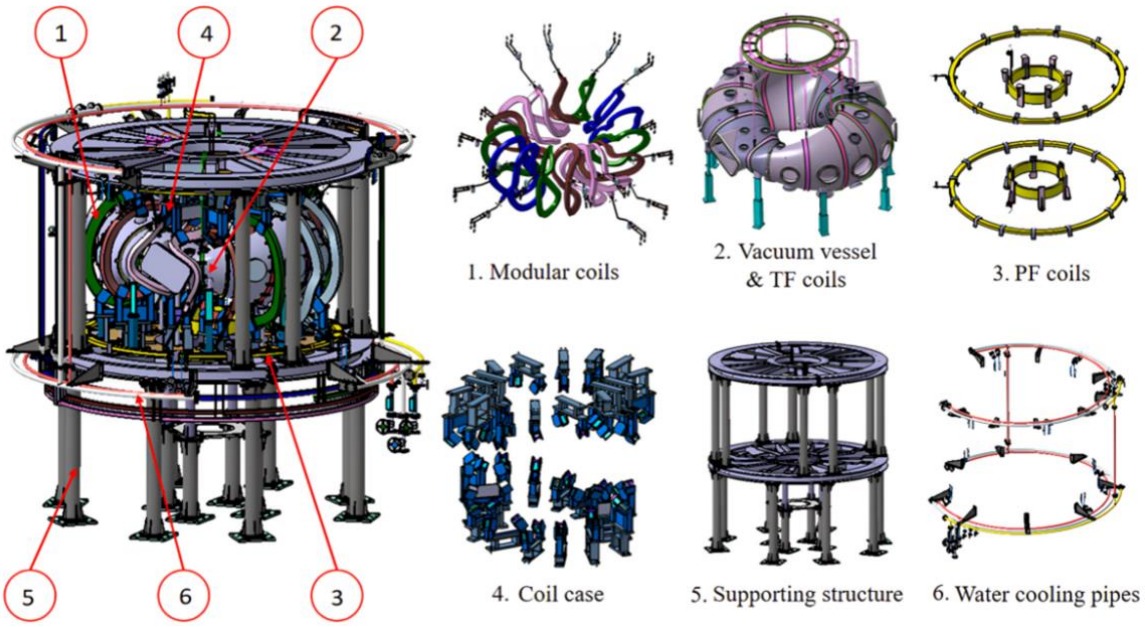

Fig. 3. Schematic of the CFQS main body, including non-planar modular coils ①, vacuum vessel together with toroidal field (TF) coils ②, poloidal field (PF) coils ③, coil cases ④, supporting structure ⑤ and water cooling pipes ⑥.

MC coils are the most complex and difficult to manufacture (see Fig. 4(a)). The first step for manufacturing the MCs is making the coil winding. The cross-sectional dimensions of the modular coil are 12 turns × 6 turns (132 mm × 69 mm), as shown in Fig. 4(b). Each coil is wound with two layers, 12 turns per layer, with an S-shaped crossover between layers for transition. Consequently, the coil cross section contains a total of 72 turns of copper block. Each conductor features a square outer section (8.5 mm × 8.5 mm) with a central ϕ 4 mm water-cooling hole. After winding, the vacuum pressure impregnation (VPI) is performed twice to fix and insulate the copper conductors. Finally, the dimension measurement is done by the laser tracker to check the achieved accuracy of the MCs. Figure 5 displays

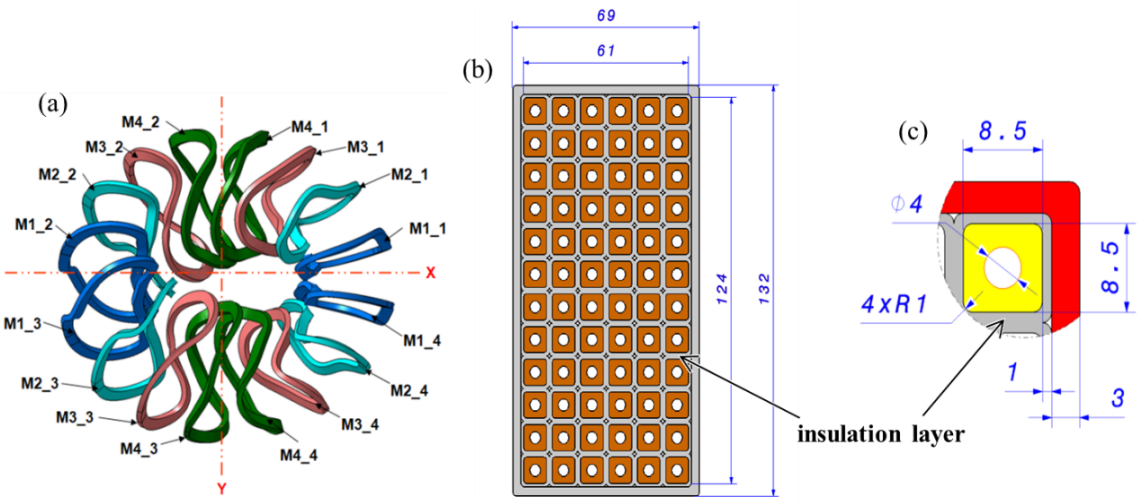

Fig. 4. (a) Top view of 16 MC coils (MC1-MC4 of 4 types), (b) cross-section of the MC coil and (c) dimension and structure of one turn.

the manufactured MCs, PFCs and TFCs. Detailed parameters for the CFQS coil system can be found in ref. [15]. **The vacuum vessel (VV)** is one of the main components of the CFQS device. Plotted in Fig. 6(a) is the schematic view of VV, which is composed of four sections (2×type A and 2×type B) and all these sections are weld one by one in the toroidal direction. Shown in Figs. 6(b)-(c) are the fabrication details for type A and type B, which are weld by four and seven pieces of 6 mm thick stainless steel plate (SUS316L), respectively. The final pictures of the fabricated type A and B are shown on the right side of Fig. 6. Then, the VV wall was baked by the resistance wires, which are distributed on the VV surface at the temperature of 130 ~150 °C [16]. ANSYS simulation results indicate that the maximum stress and

Fig. 5. (a) Photos for the manufactured MC coils, (b) PFC (inner vertical/outer vertical) coils and (c) TFC coils wound on the vacuum vessel surface.

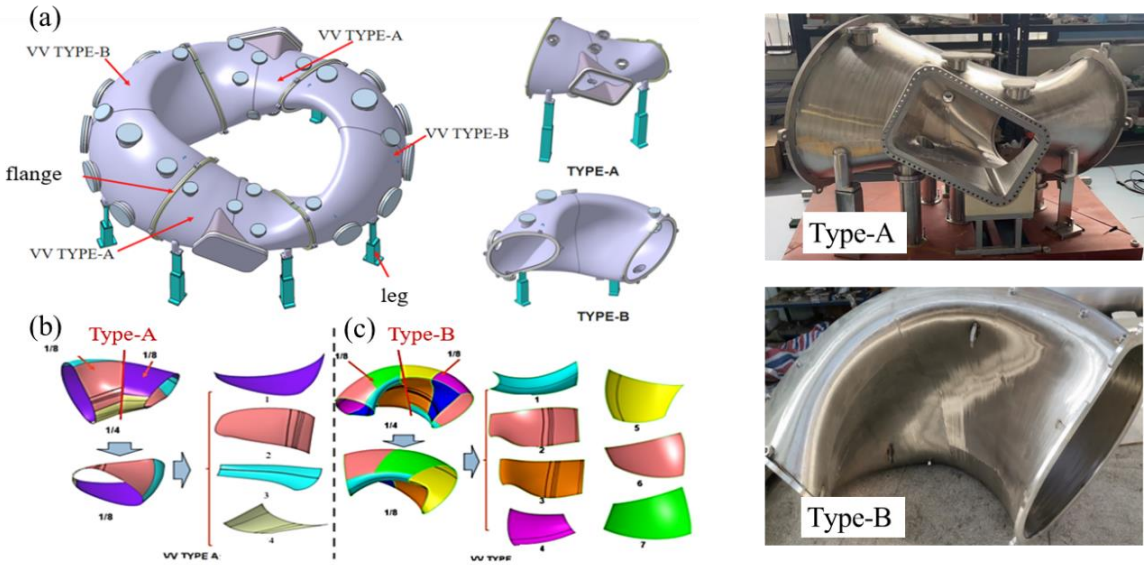

Fig. 6. (a) Schematic view of vacuum vessel including four toroidal sections (2 for type A and 2 for type B), (b) type A and type B are fabricated by four pieces and seven pieces of 6 mm thick stainless steel plates, respectively. Shown at the right side are photos of fabricated type A and B.

deformation are 126 MPa and 3 mm respectively, which are below allowable level [17]. For the CFQS-T operation at $B_t = 0.1$ T, **the support structure** could resist the electromagnetic force without coil case and it could also reduce the deformation via the coil own stiffness, thus this structure can be used for low magnetic field experiments of 0.1 T. For CFQS with $B_t = 1$ T operation, the strong electromagnetic force will impose on the MC coils, a dedicated support structure, including coil cases, center pole and pillars between adjacent modular coils, is designed for reinforcement of modular coils [16]. Analysis based on the finite element method has been performed to check the stress, deformation and elastic strain. The results show that the designed support structure is capable of resisting the strong electromagnetic force in CFQS with 1 T operation [18]. After the assembly of all coils including MC, PFC, and TFC as well as vacuum sections and pillars in CFQS-T, the maximum deviation of the MC position is about 2.96 mm (see Fig. 7), meeting the design requirement [16, 19]. The resultant error of the magnetic configuration is around 10^{-4} ($\delta b_{52}/B_0=1.1\times10^{-4}$, where δb_{52} is the deviation at m/n=5/2 island) [20], which is also below the allowable level.

Assembly of CFQS-T device was carried out in several stages, i. e., installation of 2 lower PFCs, MCs and vacuum vessel sections (type A/B) threaded through the 16 MCs, followed by mounting 8

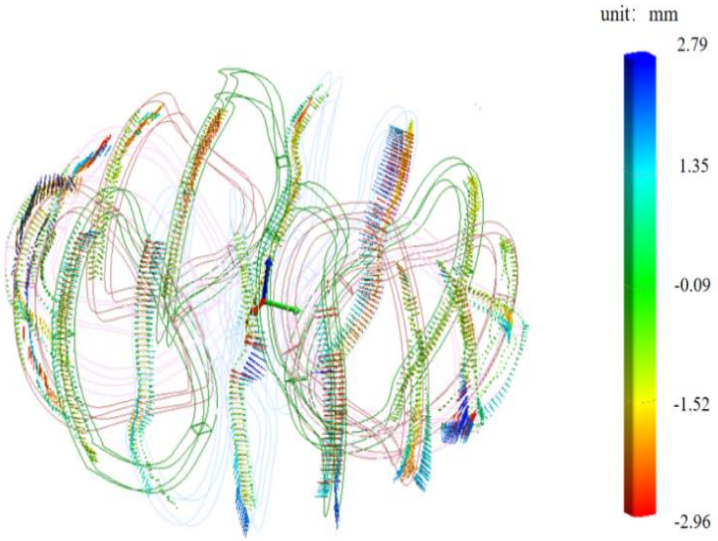

Fig. 7. The dimension measurement for the entire MC coils of the CFQS-T device, where the color denotes deviation of MC positions from a 3D CAD model.

outer pillars, 2 upper PFCs, 12 TFCs and water pipes. In each stage, the positioning of the coils was kept by precision laser tracker. By the end of July 2024, the assembly of CFQS-T was completed. The auxiliary systems, including power supply, vacuum pumping, magnetron (2.45 GHz, 10-30 kW), central control, gas puff and diagnostic systems, have also been installed and commissioned accordingly.

3. Preliminary experimental results on the CFQS-Test device

In August of 2024, the first QA magnetic configuration was successfully achieved in CFQS-T. Figure 8 illustrates the mapping system used to measure the magnetic topology along with the 2D and 3D structures of the magnetic surfaces. Figure 8(a) shows that the mapping diagnostic mainly consists of three elements: an electron gun (energy range: 20-250 eV), a fluorescent mesh (grid size: 2 cm × 2

cm) and a high-sensitivity camera (exposure time: ~ 60 s) [21]. The electron beam emitted from the electron gun at a fixed radial position travels along the magnetic field lines. When it strikes the

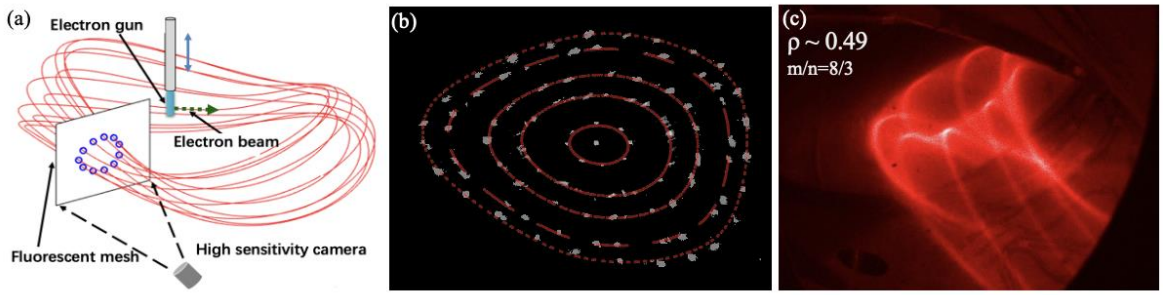

Fig. 8. (a) Schematic of mapping system; (b) 2D Poincare section of closed magnetic surfaces measured by fluorescent mesh and (c) 3D structure of magnetic field lines visualized in argon gas.

fluorescent mesh, the latter will light up. The illuminated pattern is continuously recorded by the high-sensitivity camera. By emitting the electron beam at different radii, various magnetic surfaces can be visualized. The mapping results are shown in Fig. 8(b), where the white light points clearly show Poincare section of nested and closed flux surfaces, in good agreement with the simulated values (red curves) [10, 13]. Besides, the electron beam alone could also visualize the 3D structure of field lines via collisional excitation of argon gas, as shown in Fig. 8(c) with a striking image of the m/n = 8/3 modes. Using the method proposed by Boozer [22], the error field of intrinsic 5/2 island is evaluated to be ~ 5.6×10^{-5}, meeting our design request. The first plasma was successfully achieved on the CFQS-T

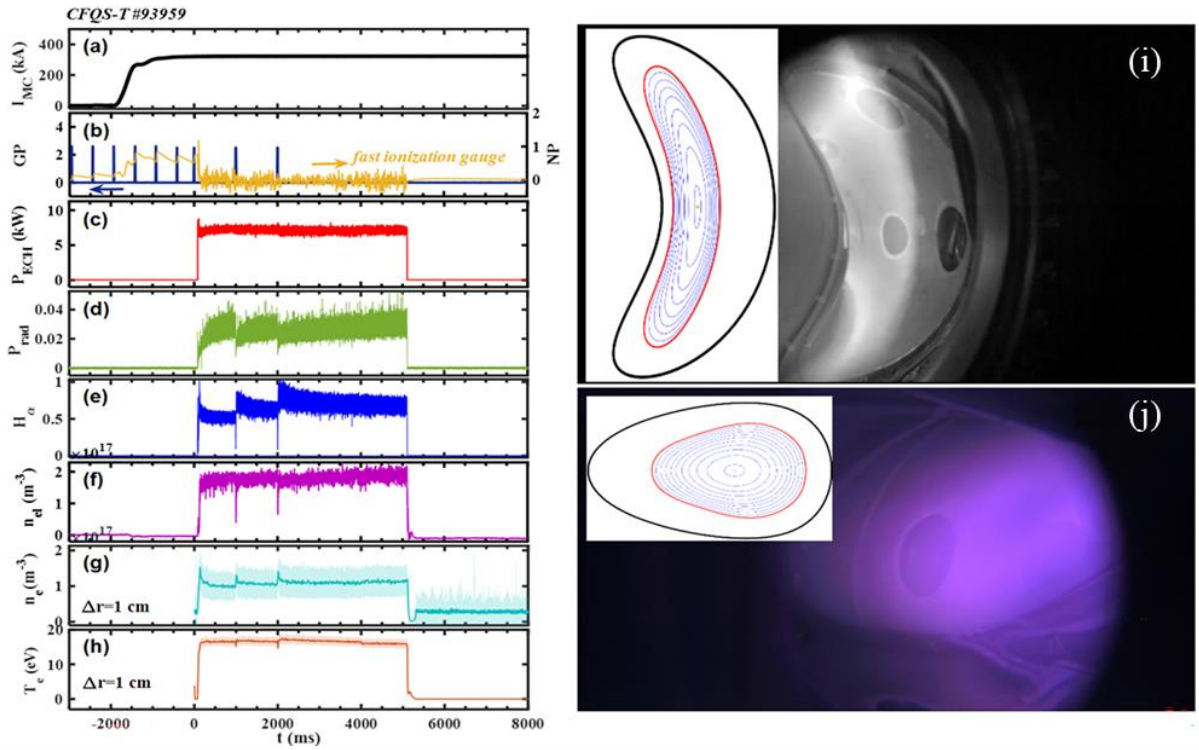

Fig. 9. Time traces of (a) MC currents, (b) gas puffing pulses and neutral gas pressure, (c) heating power, (d) total radiated power, (e) H_α emission intensity, (f) line-averaged density, (g) the electron density and (h) temperature measured by the stationary Langmuir probe located at SOL (Δ r=1 cm). Shown at right side are plasma shapes captured by CCD at toroidal 0 (i) and 90 degrees (j), respectively.

device in August of 2024. Shown in Figs. 9(a)-(h) are the typical discharge waveforms, including the MC coil currents, hydrogen gas pulses together with fast ionization gauge, magnetron power, plasma radiation measured by bolometer, H_α emission, the line-averaged density measured by microwave interferometer and electron temperature and density measured by a stationary Langmuir probe located at the scrape-off layer ($\Delta r \approx 1$ cm) calculated by the VMEC code [12]. At approximately $t = -3$ s, gas puffing is pulse injected for the increase of neutral gas, and then the QA magnetic configuration is formed at about $t = -1$ s. Then, the plasma start-up occurs at $t = 0$ s, which is triggered by the magnetron heating. At the same time, one can see that the plasma radiation, the H_α emission, the line-averaged density and the electron temperature and density measured by the stationary Langmuir probe ($\Delta r \approx 1$ cm) all rise accordingly. The maximum discharge time could reach about 10 s. The distinctive plasma shapes, captured by the CCD camera at toroidal 0 and 90 degree, are clearly visualized in Figs. 9(i)-(j), respectively.

In order to evaluate the confinement property of CFQS, a comparative study has been implemented between the CFQS and an unoptimized stellarator. Figure 10 compares the radial profiles of plasma density and electron temperature measured in CFQS-T with those in a conventional stellarator, Compact Helical System (CHS) under similar discharge and heating conditions [23]. Figure 10(a) shows that in CFQS-T the electron temperature reached up to $T_e \approx 35$ eV in the plasma core, and the electron density reached a peak value of $n_e \approx 8\times10^{17}$ m^{-3}, which are much higher (roughly four times denser and twice hotter) than those obtained in CHS. Further quantitative assessment using the SFINCS code [24] reveals that the neoclassical electron flux (Γ_e) and normalized heat flux ($V'Q_{neo}/P_{heat}$) are both reduced remarkably in the CFQS-T [25]. These results show clear evidence of better particle confinement being achieved in an optimized QA configuration, consistent with our expectation.

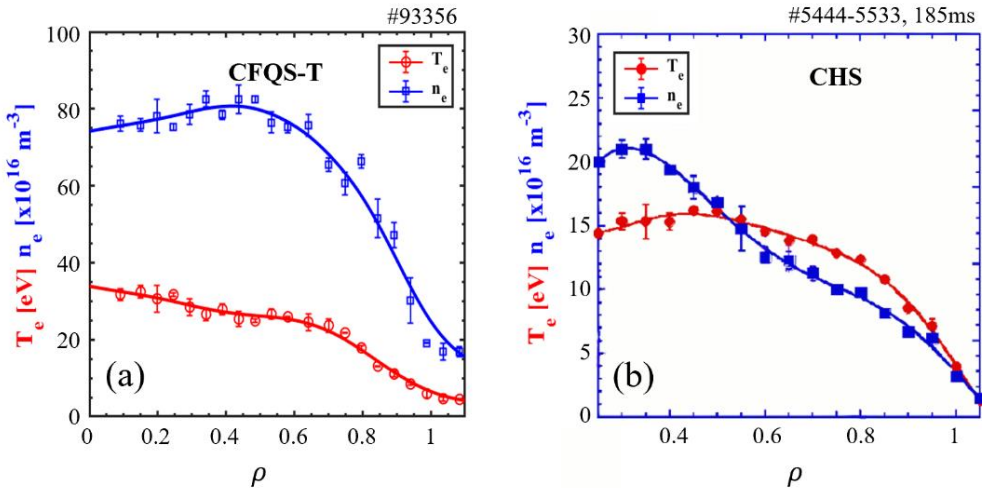

Fig. 10. Comparison of electron temperature (T_e) and density (n_e) profiles between (a) CFQS-T and (b) CHS under similar discharge condition (H plasma, $B_t \sim 0.06$ T) and heating power (ECRH, ~ 10 KW, 2.45 GHz).

4. Summary

In this paper, we have reported the construction progress of CFQS and the preliminary experimental results obtained in the CFQS-T device. The results, **for the first time**, validate the accurate QA magnetic topology in the CFQS-T stellarator with modular coils **in the world**, and demonstrate the capability of

the optimized QA configuration in trimming down the neoclassical transport. Further analyses of plasma properties, such as turbulent transport and MHD activities, are being underway.

References:

[1] Galeev A A 1969 *Phys. Rev. Lett.* 22 511

[2] Nührenberg J 1988 *Phys. Lett. A* 129 113

[3] Helander P *et al* 2014 *Rep. Prog. Phys.* 77 087001

[4] Zarnstorff M *et al* 2001 *Plasma Phys. Control. Fusion* 43 A237

[5] Xu Y et al, 27th IAEA Fusion Energy Conference (Ahmedabad, 2018), EX/P5-23

[6] Isobe M *et al* 2019 *Plasma Fusion Res.* 14 3402074

[7] Okamura S *et al* 2004 *Nucl. Fusion* 44 575

[8] Xu Y *et al* 2016 *Matter Radiat. Extremes* 1 192

[9] Shimizu A *et al* 2018 *Plasma Fusion Res.* 13 340323

[10] Liu H F *et al* 2021 *Nucl. Fusion* 61 016014

[11] Kinoshita S *et al* 2019 *Plasma Fusion Res.* 14 3405097

[12] Liu H F *et al* 2018 *Plasma Fusion Res.* 13 3405067

[13] Shimizu A *et al* 2022 *Nucl. Fusion* 62 16010

[14] Okamura S *et al* 2020 *J. Plasma Phys.* 86 815860402

[15] Cheng J, Xu Y, Liu H F *et al* 2025 *Plasma Phys. Control. Fusion*, in press.

[16] Kinoshita S *et al* 2019 *Plasma Fusion Res.* 14 3405097

[17] Nakagawa S *et al* 2020 *Plasma Fusion Res.* 15 2405066

[18] Xiong G Z *et al* 2020 *Fusion Eng. Des*. 160 112021

[19] Xiong G Z *et al* 2023 *Plasma Phys. Control. Fusion* 65 035020

[20] Li D *et al* 2025 *Acta Physica Sinica* 74 055203

[21] Shoji M *et al* 2023 *Plasma Fusion Res.* 18 2405026

[22] Boozer A H *et al* 2015 *Nucl. Fusion* 55 025001

[23] Ikeda R and Takeuchi M, 2006 *Journal of the Korean Physical Society* 49 S206-210

[24] Landreman M *et al* 2014 *Physics of Plasmas* 21 042503

[25] Xu Y *et al* 2025 to be submitted to *Nature Physics*